Interface-relevant out-of-plane spin polarization in $IrMn_3$/permalloy bilayers

Shixuan Liang,* Lei Han,* Yunfeng You, Hua Bai, Feng Pan, and Cheng Song†
Key Laboratory of Advanced Materials (MOE), School of Materials Science and Engineering, Tsinghua University, Beijing 100084, China

(Received 4 February 2023; revised 25 April 2023; accepted 26 April 2023; published 12 May 2023)

Out-of-plane spin polarization (σ_z) has potential applications for magnetic memory with high storage density and low energy consumption. Several noncollinear antiferromagnets have been confirmed to generate σ_z due to their triangular spin configuration on kagome planes, including $IrMn_3$. Apart from the spin configuration of the (110)-oriented $IrMn_3$, we demonstrate that the interface of $IrMn_3$/permalloy also contributes to the generation of σ_z. With Cu insertion between $IrMn_3$ and permalloy, interfacial σ_z vanishes, which further supports the interfacial origin of σ_z. We are not only convinced that the interface-relevant σ_z is independent of exchange coupling between $IrMn_3$ and permalloy but also propose several possible origins of interface-relevant σ_z. Our findings enrich the understanding of generating σ_z in antiferromagnets/ferromagnets bilayers. The interface-relevant σ_z broadens the scope of material design and proposes a potential path to optimize magnetic memories with low power consumption.

DOI: 10.1103/PhysRevB.107.184427

I. INTRODUCTION

According to the classic scenario of spin-orbit torque (SOT) induced by the spin Hall effect (SHE), a charge current flowing in the in-plane direction (x axis) generates a spin current along the out-of-plane direction (z axis) with spin polarization along the y axis (σ_y) [1,2]. In this case, ferromagnets (FM) with perpendicular magnetic anisotropy, which benefit high-density storage and device miniaturization, usually need an external magnetic field to break the symmetry in order to achieve deterministic switching [3–7]. Recently, out-of-plane spin polarization (σ_z) has received a great deal of interest due to its ability to realize field-free switching of perpendicular magnetization with high efficiency [8–10]. In general, σ_z can be generated not only from nonmagnets (NM) with low crystalline symmetry [8,11–13], but also from several antiferromagnets (AFM) owing to the reduced symmetry considering the magnetic structure [14–22]. The noncollinear antiferromagnet $IrMn_3$ has compensated moments with 120° triangular spin texture in the {111} kagome plane as shown in Fig. 1(a) [17], giving rise to nontrivial magnetoelectrical transport phenomena [23,24]. Previous studies have reported that $IrMn_3$(100) can generate σ_z and corresponding unconventional torques, making $IrMn_3$ a promising spin source [17,18].

Interfaces play a pivotal role in SOTs. In addition to the σ_y from the Rashba-Edelstein effect [3,25–27], σ_z has also been investigated at the FM/NM interface. The origin of σ_z includes the spin-orbit precession due to the interfacial spin-orbit field [28], anomalous SHE [29], magnetization-dependent SHE [30,31], and nonequilibrium spin swapping [32]. Compared with FM, AFM has vanishing magnetization with fast dynamics and negligible stray field [33,34]. Moreover, the magnetic structure of AFM may bring about a new dimension for the interface-relevant σ_z. However, the generation of σ_z at AFM/FM interfaces still remains elusive.

In this work, we demonstrate (110)-oriented $IrMn_3$ can generate out-of-plane fieldlike torques relevant to the $IrMn_3$/Permalloy ($Ni_{80}Fe_{20}$, Py) interface as well as the bulk of $IrMn_3$ via spin-torque ferromagnetic resonance (ST-FMR) measurements. Figure 1(b) shows the bulk origin of σ_z that relates to the spin configuration of $IrMn_3$. When the applied current ($\boldsymbol{J_c}$) is parallel to the cluster magnetic octupole moment ($\boldsymbol{T}$), spins will precess along the spin-orbit field ($\boldsymbol{H}_{SO}$) produced by the current, bringing about out-of-plane components. Besides the bulk of $IrMn_3$, the interface of $IrMn_3$/Py can generate σ_z even though $\boldsymbol{J_c} \perp \boldsymbol{T}$, as displayed in Fig. 1(c). In the $IrMn_3$/Cu/Py control sample, the vanishment of σ_z further reveals the relevance between the additional σ_z and the $IrMn_3$/Py interface. After performing the field annealing, the interface-relevant σ_z degenerates while the bulk-induced σ_z keeps still no matter which direction the annealing field is along.

II. EXPERIMENTS

We grew 23-nm-thick $IrMn_3$ (110) films on MgO (110) substrates at 773 K by DC magnetron sputtering followed by 1-h annealing at 773 K *in situ*. X-ray-diffraction spectrum of $IrMn_3$ indicates obvious peaks of $IrMn_3$ (110) and (220), apart from the peaks of MgO (220) as shown in Fig. 1(d). Secondary phases do not emerge in the present $IrMn_3$ (110). Figure 1(e) shows the Φ-scan measurement of $IrMn_3$ {100} and MgO {100} at $\chi = 45°$, confirming the quasiepitaxial growth mode of $IrMn_3$. The crystallographic orientation of $IrMn_3$ relative to the substrate is epitaxial $IrMn_3$ $\{110\}\langle100\rangle \parallel$ MgO$\{110\}\langle100\rangle$, demonstrated by the same peak position of $IrMn_3$ and MgO substrate. Magnetic hysteresis loop measured by the superconducting quantum interference device (SQUID)

*These authors contributed equally to this work.
†songcheng@mail.tsinghua.edu.cn

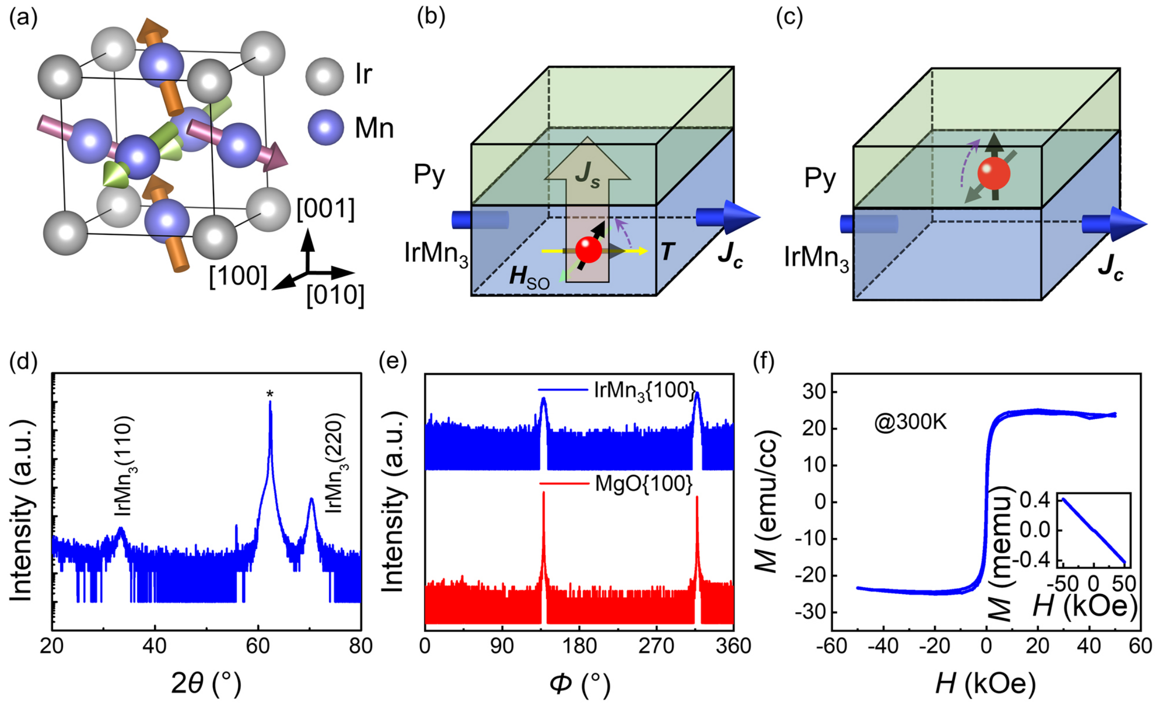

FIG. 1. Schematic of dual generation of out-of-plane spin polarization and basic properties of $IrMn_3$ film. (a) Magnetic structure of $IrMn_3$. (b) Schematic diagram of σ_z related to the relative orientation between the applied current $\boldsymbol{J_c}$ and the cluster magnetic octupole moment $\boldsymbol{T}$. (c) Schematic diagram of σ_z related to the interface of $IrMn_3$/Py. (d) θ-2θ measurement of $IrMn_3$, indicating the strong (110) orientation of $IrMn_3$ film. (e) Φ-scan measurement of $IrMn_3$ (110), demonstrating the quasiepitaxial growth mode of $IrMn_3$. (f) Magnetic hysteresis loop of $IrMn_3$ measured by SQUID. The inset is the raw data, appearing as a diamagnetic behavior with a kink around the zero field.

at 300 K with an in-plane magnetic field is shown in the inset of Fig. 1(f), appearing as a diamagnetic behavior with a tiny kink around zero field, which indicates the antiferromagnetic characteristic of $IrMn_3$. For better understanding, the diamagnetic base is deducted in Fig. 1(f). Saturated magnetization is around 24 emu/cc, which is reasonable in noncollinear antiferromagnets [19,35]. The prepared $IrMn_3$ films with strong (110) orientation provide a precondition for further study of charge-to-spin conversion.

We deposited 15-nm-thick Py and 2-nm-thick Al on the (110)-oriented 12-nm-thick $IrMn_3$ after cooling to the room temperature *in situ*. $IrMn_3$/Py/Al samples were patterned into microstrips with a size of 30 μm × 20 μm by standard photolithography and Ar-ion milling techniques. Top electrodes of Ti/Au were then deposited by e-beam evaporation. Devices with different orientations were fabricated to investigate the symmetry of the generation of σ_z. The current direction in conjunction with the cluster magnetic octupole moment can be controlled by choosing different ST-FMR devices.

ST-FMR was used to measure the spin torques in $IrMn_3$/Py bilayers. As shown in Fig. 2(a), microwave current was applied along the stripe, which arouses an alternating torque on the upper Py with the same period as the rf current. Successively, the precession of magnetic moments in Py excited by the rf current drives the resistance of the stripe to change periodically due to the anisotropy magnetoresistance. Mixing with the alternating current through Py, alternating resistance generates a double-frequency voltage signal as well as zero-frequency signal, namely, the rectified voltage V_{mix} which is measured by a nanovoltmeter.

III. RESULTS AND DISCUSSION

The discussion of ST-FMR spectrum is based on the V_{mix} as a function of the external magnetic field H shown in Fig 2. At a fixed frequency, V_{mix} around the resonance magnetic field H_{res} can be fitted as a function of magnetic field H by [36]

$$V_{mix} = V_S \frac{\Delta H^2}{\Delta H^2 + (H - H_{res})^2} + V_A \frac{\Delta H (H - H_{res})}{\Delta H^2 + (H - H_{res})^2}, \tag{1}$$

where H_{res} is the resonance magnetic field, and ΔH is the linewidth. The amplitude of the Lorentzian symmetric line shape V_S and the antisymmetric V_A is proportional to the amplitude of the in-plane torque $\tau_\parallel$ and out-of-plane torque $\tau_\perp$, respectively, as illustrated in Fig 2(a). Note that the angle between the applied current $\boldsymbol{J_c}$ and the magnetic field $\boldsymbol{H}$ is denoted by φ_H. Figure 2(b) displays the measured V_{mix} at $\varphi_H = 40^\circ$, 10 GHz, and 15 dBm in $IrMn_3$/Py, where the applied current is along the $[1\bar{1}0]$ crystal axis of $IrMn_3$. Note that the materials with high symmetry only allow conventional torques corresponding to SHE or the Rashba-Edelstein effect, where $V_{mix}(H)$ should be equal to $-V_{mix}(-H)$. Strikingly, the amplitude of V_S in the positive field is much larger than that in the negative field in $IrMn_3$/Py as depicted in Fig. 2(b), revealing the unconventional torque triggered by σ_z. Then, $4\pi M_{eff}$ is extracted from the Kittel equation $f = \frac{\gamma}{2\pi}\sqrt{H_{res}(H_{res} + 4\pi M_{eff})}$ in Fig. 2(c), whose value is 9320 Oe, indicating the resonance peak originates from the ferromagnetic resonance signal of Py.

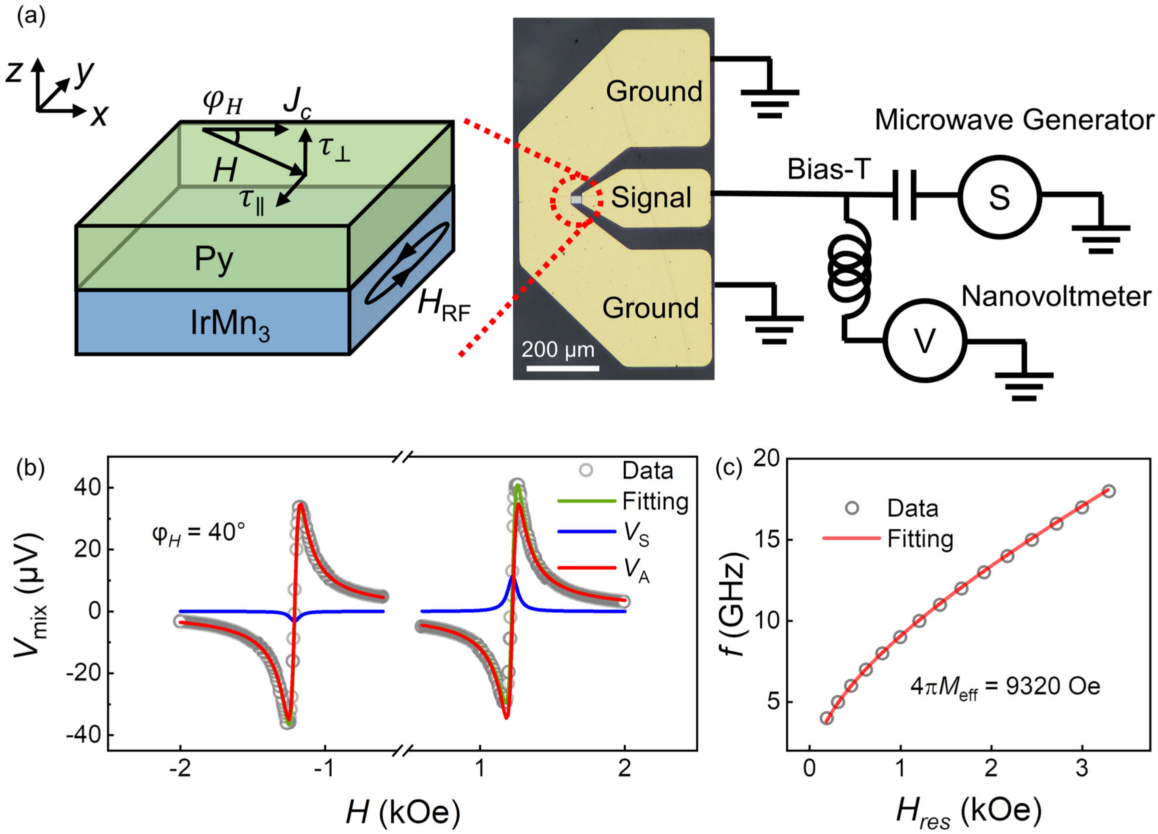

FIG. 2. ST-FMR measurement of $IrMn_3$/Py. (a) Schematic of ST-FMR geometry of $IrMn_3$/Py bilayer, corresponding optical microscope graph of the device, and the setup. φ_H is the angle between rf current $\boldsymbol{J_c}$ and magnetic field $\boldsymbol{H}$. rf current is triggered in microwave generator and the rectified voltage is measured by nanovoltmeter. (b) ST-FMR spectrum of $IrMn_3$/Py at 10 GHz and $\varphi_H = 40^\circ$. Raw data V_{mix} are shown as gray circles, while the fitting line is depicted in green. V_S and V_A extracted from fitting lines are illustrated in blue and red, respectively. (c) Frequency fitting of Kittel equation from 4 to 18 GHz at $\varphi_H = 45^\circ$ and the corresponding M_{eff}. Resonance field H_{res} is extracted from the fitting of V_{mix} likewise.

f, γ, and M_{eff} are the microwave frequency, the gyromagnetic ratio, and the effective magnetization, respectively.

To investigate the components of the torque generated by $IrMn_3$, angular-dependent ST-FMR measurements are performed. Antidamping torques exhibit a common form of $\boldsymbol{\tau}_{AD} \propto \boldsymbol{m} \times \boldsymbol{\sigma} \times \boldsymbol{m}$, in which $\boldsymbol{\sigma}$ is the spin polarization and $\boldsymbol{m}$ stands for the unit vector of magnetization. The common form of fieldlike torques is $\boldsymbol{\tau}_{FL} \propto \boldsymbol{m} \times \boldsymbol{\sigma}$. The direction of $\boldsymbol{\sigma}$ determines the variation of corresponding torques with φ_H. The spin polarization along the x axis (σ_x), σ_y, and σ_z contribute to $\sin\varphi_H \sin 2\varphi_H$, $\cos\varphi_H \sin 2\varphi_H$, and $\sin 2\varphi_H$ components, respectively. By fitting V_S and V_A as a function of φ_H, components of torques triggered by $IrMn_3$ can be differentiated individually. V_S and V_A can be expressed, respectively, as

$$V_S = \tau_{AD,\,x} \sin\varphi_H \sin 2\varphi_H + \tau_{AD,\,y} \cos\varphi_H \sin 2\varphi_H + \tau_{FL,\,z} \sin 2\varphi_H, \quad (2)$$

$$V_A = \tau_{FL,\,x} \sin\varphi_H \sin 2\varphi_H + \tau_{FL,\,y} \cos\varphi_H \sin 2\varphi_H + \tau_{AD,\,z} \sin 2\varphi_H, \quad (3)$$

where $\tau_{AD,x}$, $\tau_{AD,y}$, and $\tau_{AD,z}$ are the coefficients related to antidamping torques. Likewise, $\tau_{FL,x}$, $\tau_{FL,y}$, and $\tau_{FL,z}$ are the coefficients corresponding to fieldlike torques. Given that fieldlike torques triggered by σ_y have the same symmetry, $\cos\varphi_H \sin 2\varphi_H$, but a negligible amplitude compared with torques generated by the Oersted field, $\tau_{FL,y}$ is considered as the contribution from Oersted field [36,37]. V_A can be well fitted by $\cos\varphi_H \sin 2\varphi_H$ in each device, indicating that V_A is mainly contributed by the Oersted field (Fig. S1 in Supplemental Material [38]). Hence, only V_S is shown and discussed in this study.

When the applied current ($\boldsymbol{J_c}$) is parallel to [001] ($\boldsymbol{J_c} \parallel \boldsymbol{T}$), the emergence of σ_z can be well interpreted by the cluster magnetic octupole ($\boldsymbol{T}$). Each cluster is defined as six Mn atoms related to each other by crystal-symmetry operators without space translation in a magnetic unit cell [39]. $\boldsymbol{T}$ can be considered as a ferroic ordering, pointing to the same direction as the tiny canted moment, illustrated by yellow arrows in Figs. 3(a) and 3(d) [14,40,41]. When the charge current is applied to $IrMn_3$, a spin-orbit field $\boldsymbol{H}_{SO}$ perpendicular to the current arises [42], making spins precess around it. The generation of σ_z depends on the conjunction between $\boldsymbol{T}$ and $\boldsymbol{J_c}$, namely, $\sigma_z \propto \boldsymbol{H}_{SO} \times \boldsymbol{T}$ [20]. The principle of generating σ_z mentioned above is equal to the magnetic symmetry analysis regarding $IrMn_3$ [17]. The magnetic mirror symmetry M' contains a crystal mirror symmetry M and a time-reversal symmetry. Although $IrMn_3$ has high crystal symmetry, even twofold

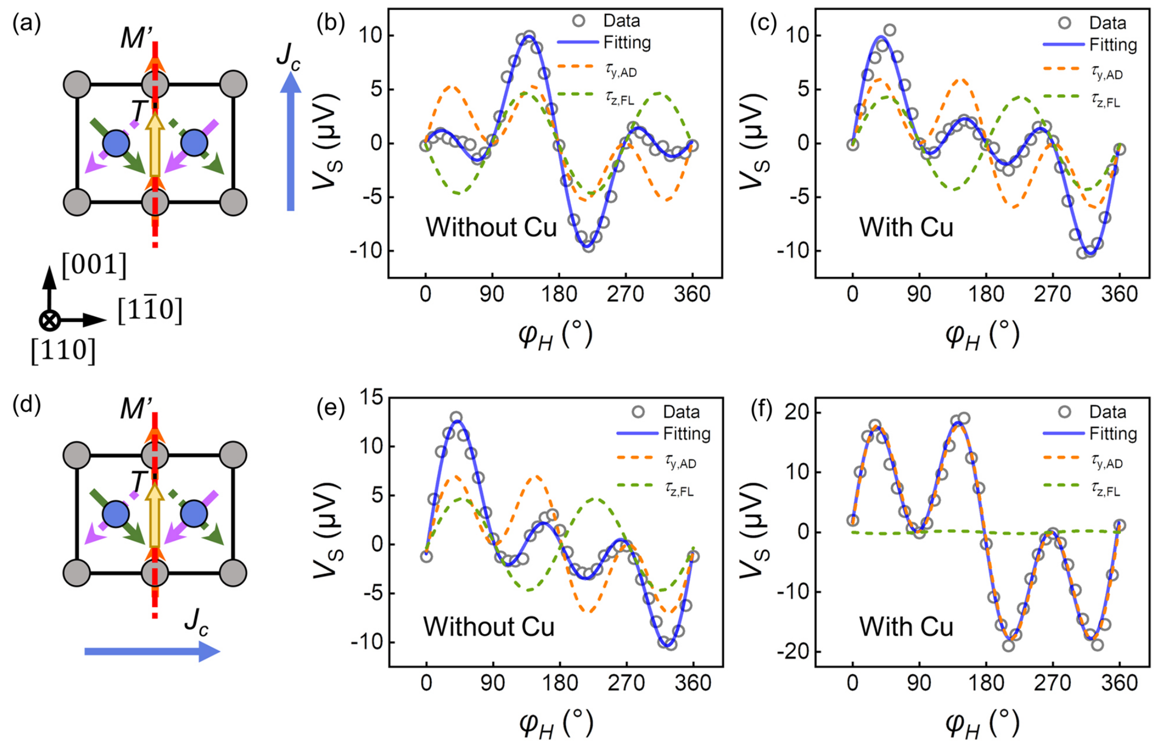

FIG. 3. V_S extracted from ST-FMR spectrum at varied φ_H in $IrMn_3$/Py and $IrMn_3$/Cu/Py. (a), (d) Projection of crystal structure and spin texture on the (110) plane. Applied current ($\boldsymbol{J_c}$) is parallel to the cluster magnetic octupole moment $\boldsymbol{T}$ (a) and perpendicular to $\boldsymbol{T}$ (d). Red dashed line indicates the magnetic mirror M'. Yellow arrow represents the direction of $\boldsymbol{T}$. Gray and blue balls denote Ir and Mn atoms, respectively. (b), (c) Angular-dependent symmetric signal and its components when $\boldsymbol{J_c} \parallel \boldsymbol{T}$ ($\boldsymbol{J_c} \parallel \boldsymbol{M'}$) without (b) or with Cu insertion (c). (e), (f) Angular-dependent V_S and its components when $\boldsymbol{J_c} \perp \boldsymbol{T}$ ($\boldsymbol{J_c} \perp \boldsymbol{M'}$) without (e) or with (f) Cu insertion.

rotational variation is lost if taking the magnetic structure of $IrMn_3$ into consideration. The magnetic mirror symmetry is broken on condition that $\boldsymbol{J_c} \parallel \boldsymbol{M'}$, which triggers σ_z. The magnetic mirror M' in $IrMn_3$ is parallel to the (1$\bar{1}$0) plane, whose projection is indicated as red dashed lines in Figs. 3(a) and 3(d). Note that the arrows through the blue balls denote the magnetization of each Mn atom. Arrows with the same color indicate the same direction, and atoms with solid arrows are above those with dashed arrows. (See 3D structure of M' and T in Fig. S3 in the Supplemental Material [38].) In Fig. 3, the angle-dependent V_S can be well fitted by the sum of $\cos\varphi_H \sin 2\varphi_H$ and $\sin 2\varphi_H$, which are corresponding to the antidamping torque generated by σ_y ($\tau_{AD,\,y}$) and the fieldlike torque generated by σ_z ($\tau_{FL,\,z}$), respectively. If $\boldsymbol{J_c} \parallel \boldsymbol{T}$ ($\boldsymbol{J_c} \parallel \boldsymbol{M'}$) as shown in Fig. 3(b), $\tau_{FL,\,z}$ has a comparable amplitude with $\tau_{AD,\,y}$, showing the robust emergence of σ_z in $IrMn_3$/Py, which is consistent with the principle above. Surprisingly, considerable σ_z still arises when $\boldsymbol{J_c} \perp \boldsymbol{T}$ ($\boldsymbol{J_c} \perp \boldsymbol{M'}$), as depicted in Fig. 3(e). To probe the derivation of the unexpected σ_z, control samples with 2-nm-thick Cu insertion between $IrMn_3$ and Py are prepared, as the long diffusion length of Cu. In $IrMn_3$/Cu/Py samples, currents applied along $\boldsymbol{T}(\boldsymbol{M'})$ can trigger σ_z as shown in Fig. 3(c) while currents perpendicular to $\boldsymbol{T}(\boldsymbol{M'})$ cannot [Fig. 3(f)]. The crystallographic orientation-dependent σ_z is consistent with previous studies in noncollinear antiferromagnets [17,19]. The Cu insertion allows the transmission of spin currents and eliminates the possible interfacial effect in the $IrMn_3$/Py bilayer. Therefore, the disappearance of σ_z with the applied current $\boldsymbol{J_c}$ perpendicular to $\boldsymbol{T}(\boldsymbol{M'})$ suggests the additional contribution to σ_z is probably related to $IrMn_3$/Py interface.

Among the interfacial effects of AFM/FM bilayers, exchange coupling between AFM and FM should be considered first, whose intensity is usually reflected by the exchange bias. We control the exchange coupling of $IrMn_3$/Py via annealing and cooling at 473 K in an in-plane magnetic field of 8 kOe. The obtained exchange bias in $IrMn_3$/Py is confirmed by the magnetization measurements (Fig. S2 in Supplemental Material [38]). Notably, $\tau_{AD,\,y}$ in $IrMn_3$/Py bilayer is attributed to the SHE due to the large spin-orbit coupling of $IrMn_3$, which has been proven to be independent of exchange coupling [43]. Considering that $\tau_{AD,\,y}$ in $IrMn_3$/Py bilayer cannot be influenced by the field annealing, hence we use $\tau_{FL,z}/\tau_{AD,y}$ to evaluate the amplitude of fieldlike torque generated by σ_z.

As for the device where $\boldsymbol{J_c} \perp \boldsymbol{T}$, $\tau_{FL,z}$ and $\tau_{AD,y}$ are acquired from the fitting of V_S as a function of φ_H on condition that the annealing field $\boldsymbol{H_{FA}}$ is applied along different directions, as depicted in Fig. 4. After carrying out the field annealing, $\tau_{FL,z}/\tau_{AD,y}$ declines significantly. Compared with the considerable amplitudes of $\tau_{FL,z}/\tau_{AD,y}$ in Fig. 3(e),the amplitude of $\tau_{FL,z}$ (shown as green dashed lines) is much lower than that of $\tau_{AD,y}$ (shown as orange dashed lines) in Figs. 4(a)–4(c), indicating the negligible σ_z in $IrMn_3$/Py when $\boldsymbol{J_c} \perp \boldsymbol{T}$ after field annealing. Note that the annealing fields $\boldsymbol{H_{FA}}$ are parallel to the applied current $\boldsymbol{J_c}$ with opposite directions in Figs. 4(a) and 4(b). Despite the sign of $\tau_{FL,z}/\tau_{AD,y}$ in Fig. 4(b) being opposite after $\boldsymbol{H_{FA}}$ switches, the amplitudes of $\tau_{FL,z}$ are both negligible compared with those of $\tau_{AD,y}$, indicating the

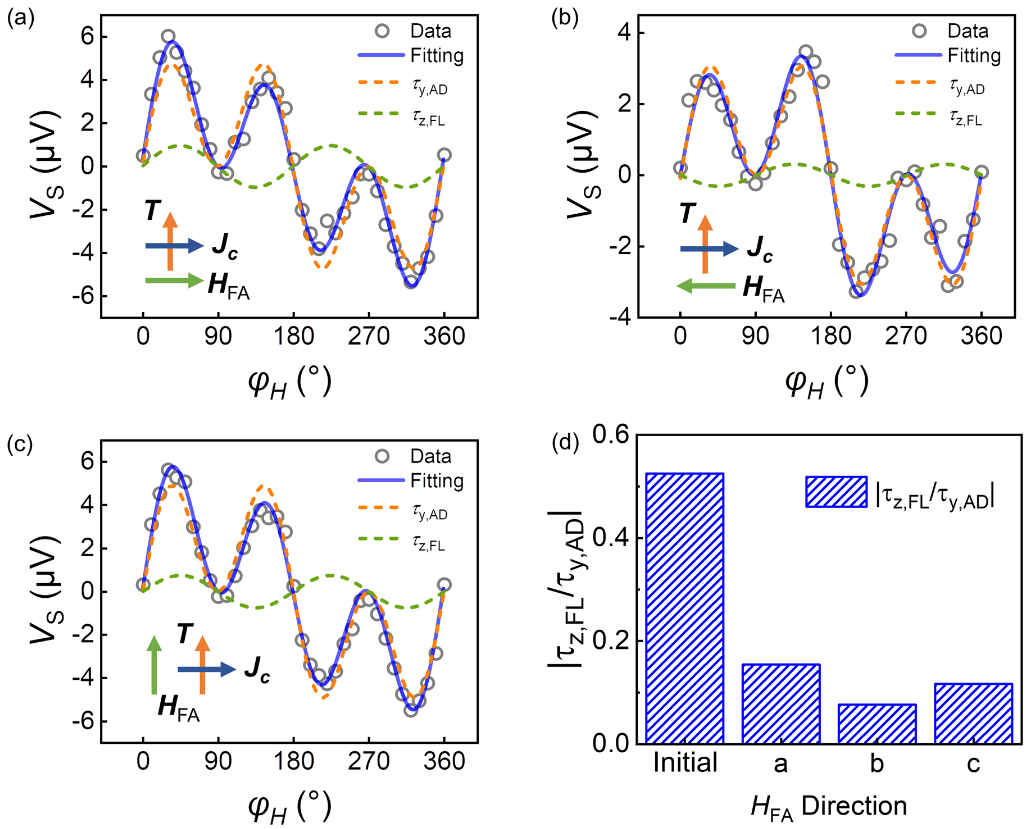

FIG. 4. Angular-dependent V_S and its components with the current $\boldsymbol{J_c}$ applied perpendicular to the cluster magnetic octupole moment $\boldsymbol{T}$ after field annealing in $IrMn_3$/Py. (a), (b) Annealing field $\boldsymbol{H_{FA}}$ perpendicular to $\boldsymbol{T}$ while parallel or antiparallel to $\boldsymbol{J_c}$, respectively. (c) Annealing field $\boldsymbol{H_{FA}}$ parallel to $\boldsymbol{T}$ while perpendicular to $\boldsymbol{J_c}$. (d) Summary of $\tau_{FL,z}$ calibrated by $\tau_{AD,y}$ in different annealing conditions.

irrelevant between generating σ_z and the sign of exchange-bias field. Similarly, the exchange-bias field perpendicular to the applied current $\boldsymbol{J_c}$ cannot make σ_z recurrent as shown in Fig. 4(c). The absolute value of $\tau_{FL,z}/\tau_{AD,y}$ is summarized in Fig. 4(d). The considerable decline of σ_z probably results from the disappearance of perpendicular moments at the interface during the field annealing, which will be discussed below. The degeneration of σ_z suggests that the in-plane exchange bias has no significant influence on the generation of σ_z relevant to the interface.

Field annealing was carried out on devices where $\boldsymbol{J_c} \parallel \boldsymbol{T}$ to probe the influence of in-plane exchange bias on bulk σ_z induced by the magnetic structure of $IrMn_3$, as shown in Fig. 5. The angle-dependent symmetry signal V_S can be decomposed into $\cos\varphi_H \sin 2\varphi_H$ (indicating the antidamping torques contributed by σ_y) and $\sin 2\varphi_H$ (indicating the fieldlike torques contributed by σ_z), shown as orange dashed lines and green dashed lines, respectively, in Fig. 5. All of the figures show a common feature that the amplitudes of $\tau_{FL,z}$ are comparable to those of $\tau_{AD,y}$, indicating the distinguished generation of σ_z in $IrMn_3$/Py after field annealing. Nevertheless, the sign of $\tau_{FL,z}/\tau_{FL,y}$ remains negative in all of the configurations. Considering the significant decline of interfacial σ_z after field annealing (Fig. 4), σ_z in cases of $\boldsymbol{J_c} \parallel \boldsymbol{T}$ (Fig. 5) is mainly from the spin configuration of $IrMn_3$, namely, the cluster magnetic octupole moments $\boldsymbol{T}$ of $IrMn_3$.

As depicted in Figs. 5(a) and 5(b), both the amplitude and the sign of σ_z have no significant change regardless of whether the annealing field is parallel or antiparallel to $\boldsymbol{T}$ in parallel conjunction with $\boldsymbol{J_c}$. Assuming that the current direction reverses, the sign of σ_z will reverse, during which case the relative orientation between $\boldsymbol{T}$ and $\boldsymbol{J_c}$ also reverses. Thus, the inverse of $\boldsymbol{T}$ will result in the sign inverse of σ_z when the direction of $\boldsymbol{J_c}$ remains unchanged. The unchanging of σ_z in Figs. 5(a) and 5(b) indicates that the direction of the cluster magnetic octupole moment $\boldsymbol{T}$ would not be modified by field annealing at 473 K, which is relatively lower than the growing and annealing temperature *in situ*. Furthermore, as shown in Figs. 5(c) and 5(d), field annealing perpendicular to $\boldsymbol{J_c}$ as well as $\boldsymbol{T}$ has no influence on the generation of σ_z contributed by the magnetic structure of $IrMn_3$. Therefore, not only the field annealing but also the exchange coupling between $IrMn_3$ and Py would not influence the σ_z arising from the bulk of $IrMn_3$.

The interfacial σ_z can be explained by the interfacial perpendicular moment of Py due to Dzyaloshinskii-Moriya (DM) interaction [38]. The inversion symmetry is broken at the interface of $IrMn_3$/Py, bringing about the DM interaction between Mn atoms and Ni (Fe) atoms, which favors the perpendicular alignment of Mn moments and Ni (Fe) moments. Ni (Fe) moments cant to the direction normal to the kagome plane of $IrMn_3$ slightly after summing up the effective DM fields on each Ni (Fe) atom per unit cell [44]. In our case of $IrMn_3$(110)/Py, the interfacial moments of Ni (Fe) perpendicular to the kagome plane {111} give the components perpendicular to {110} planes, namely, the interfacial moments normal to the interface of $IrMn_3$/Py. Out-of-plane spin

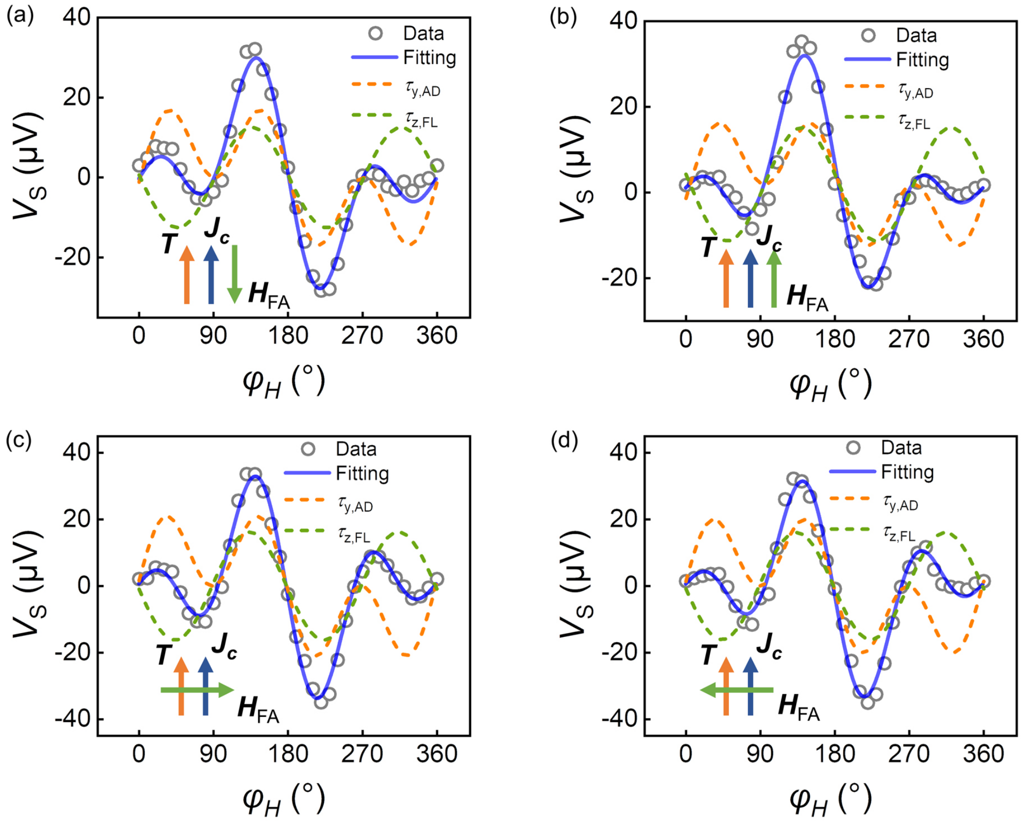

FIG. 5. Invariance of σ_z that is related to spin texture of $IrMn_3$ with the current $\boldsymbol{J_c}$ applied parallel to the cluster magnetic octupole $\boldsymbol{T}$ after field annealing in $IrMn_3$/Py. (a), (b) Annealing field $\boldsymbol{H_{FA}}$ parallel to $\boldsymbol{T}$ as well as $\boldsymbol{J_c}$. (c), (d) Annealing field $\boldsymbol{H_{FA}}$ perpendicular to $\boldsymbol{T}$ as well as $\boldsymbol{J_c}$.

polarization is generated by the exchange of the spin angular momentum between σ_y produced by the SHE of $IrMn_3$ and the interfacial moments, similar to the spin transfer in FMs [45].

Besides, the anomalous spin-orbit torque has the same form as the fieldlike torque generated by σ_z, namely, $\boldsymbol{m} \times z$ [46]. Given the strong spin-orbit coupling of $IrMn_3$, strong spin-orbit scattering arises at the $IrMn_3$/Py interface while weak scattering at Py/Al, resulting in the asymmetric anomalous spin-orbit torques at the two interfaces of Py. Hence, a net anomalous spin-orbit torque arises and may also contribute to the interface-relevant σ_z. Another possible source of interface-relevant σ_z is the nonequilibrium spin-swapping effect due to scattering related to local moments at $IrMn_3$/Py interface [32].

IV. CONCLUSION

In summary, we have investigated the dual sources of out-of-plane spin polarization in the $IrMn_3$/Py bilayer via ST-FMR. The fieldlike torque of σ_z arises in two current directions that are orthogonal to each other. The control sample with Cu insertion confirms the bulk source of σ_z related to the noncollinear spin texture of $IrMn_3$. Specifically, $\boldsymbol{J_c} \parallel \boldsymbol{T}$ triggers strong σ_z while $\boldsymbol{J_c} \perp \boldsymbol{T}$ does not in $IrMn_3$/Cu/Py. The bulk σ_z preserves its amplitude after annealing in the magnetic field; σ_z relevant to interface degenerates after the field annealing. Regardless of the direction that the in-plane annealing field is along, the amplitude of fieldlike torque related to σ_z is relatively low compared with antidamping torque related to σ_y, indicating that the interfacial σ_z is independent of the exchange coupling between $IrMn_3$ and Py. We suppose several possible origins may give rise to the interfacial σ_z at $IrMn_3$/Py interface. Our findings deepen the understanding of σ_z in noncollinear AFM/FM systems and will trigger the interests and further exploration of the derivation of interface-relevant σ_z in antiferromagnets. The interface-relevant σ_z provides potential candidates for next-generation magnetic memory devices.

ACKNOWLEDGMENTS

This work is supported by the National Key R&D Program of China (Grant No. 2021YFB3601301), the National Natural Science Foundation of China (Grants No. 52225106 and No. 12241404), and the Natural Science Foundation of Beijing, China (Grant No. JQ20010).

[1] J. Sinova, D. Culcer, Q. Niu, N. A. Sinitsyn, T. Jungwirth, and A. H. MacDonald, Universal Intrinsic Spin Hall Effect, Phys. Rev. Lett. **92**, 126603 (2004).

[2] J. Sinova, S. O. Valenzuela, J. Wunderlich, C. H. Back, and T. Jungwirth, Spin Hall effects, Rev. Mod. Phys. **87**, 1213 (2015).

[3] I. M. Miron, K. Garello, G. Gaudin, P. J. Zermatten, M. V. Costache, S. Auffret, S. Bandiera, B. Rodmacq, A. Schuhl, and P. Gambardella, Perpendicular switching of a single ferromagnetic layer induced by in-plane current injection, Nature (London) **476**, 189 (2011).

[4] L. Liu, C. Pai, Y. Li, H. W. Tseng, D. C. Ralph, and R. A. Buhrman, Spin-Torque switching with the giant spin Hall effect of tantalum, Science **336**, 555 (2012).

[5] L. Liu, O. J. Lee, T. J. Gudmundsen, D. C. Ralph, and R. A. Buhrman, Current-Induced Switching of Perpendicularly Magnetized Magnetic Layers Using Spin Torque from the Spin Hall Effect, Phys. Rev. Lett. **109**, 096602 (2012).

[6] A. Manchon, J. Železný, I. M. Miron, T. Jungwirth, J. Sinova, A. Thiaville, K. Garello, and P. Gambardella, Current-Induced spin-orbit torques in ferromagnetic and antiferromagnetic systems, Rev. Mod. Phys. **91**, 035004 (2019).

[7] C. Song, R. Zhang, L. Liao, Y. Zhou, X. Zhou, R. Chen, Y. You, X. Chen, and F. Pan, Spin-Orbit torques: Materials, mechanisms, performances, and potential applications, Prog. Mater. Sci. **118**, 100761 (2021).

[8] L. Liu, C. Zhou, X. Shu, C. Li, T. Zhao, W. Lin, J. Deng, Q. Xie, S. Chen, J. Zhou *et al.*, Symmetry-Dependent field-free switching of perpendicular magnetization, Nat. Nanotechnol. **16**, 277 (2021).

[9] S. Hu, D. F. Shao, H. Yang, C. Pan, Z. Fu, M. Tang, Y. Yang, W. Fan, S. Zhou, E. Y. Tsymbal *et al.*, Efficient perpendicular magnetization switching by a magnetic spin Hall effect in a noncollinear antiferromagnet, Nat. Commun. **13**, 4447 (2022).

[10] H. Bai, Y. C. Zhang, L. Han, Y. J. Zhou, F. Pan, and C. Song, Antiferromagnetism: An efficient and controllable spin source, Appl. Phys. Rev. **9**, 041316 (2022).

[11] D. MacNeill, G. M. Stiehl, M. H. D. Guimaraes, R. A. Buhrman, J. Park, and D. C. Ralph, Control of spin-orbit torques through crystal symmetry in WTe_2/ferromagnet bilayers, Nat. Phys. **13**, 300 (2017).

[12] M. H. D. Guimarães, G. M. Stiehl, D. MacNeill, N. D. Reynolds, and D. C. Ralph, Spin-Orbit torques in $NbSe_2$/permalloy bilayers, Nano Lett. **18**, 1311 (2018).

[13] G. M. Stiehl, D. MacNeill, N. Sivadas, I. El Baggari, M. H. D. Guimarães, N. D. Reynolds, L. F. Kourkoutis, C. J. Fennie, R. A. Buhrman, and D. C. Ralph, Current-Induced torques with Dresselhaus symmetry due to resistance anisotropy in 2D materials, ACS Nano **13**, 2599 (2019).

[14] M. Kimata, H. Chen, K. Kondou, S. Sugimoto, P. K. Muduli, M. Ikhlas, Y. Omori, T. Tomita, A. H. MacDonald, S. Nakatsuji *et al.*, Magnetic and magnetic inverse spin Hall effects in a noncollinear antiferromagnet, Nature (London) **565**, 627 (2019).

[15] X. Chen, S. Shi, G. Shi, X. Fan, C. Song, X. Zhou, H. Bai, L. Liao, Y. Zhou, H. Zhang *et al.*, Observation of the antiferromagnetic spin Hall effect, Nat. Mater. **20**, 800 (2021).

[16] T. Nan, C. X. Quintela, J. Irwin, G. Gurung, D. F. Shao, J. Gibbons, N. Campbell, K. Song, S. Y. Choi, L. Guo *et al.*, Controlling spin current polarization through non-collinear antiferromagnetism, Nat. Commun. **11**, 4671 (2020).

[17] J. Zhou, X. Shu, Y. Liu, X. Wang, W. Lin, S. Chen, L. Liu, Q. Xie, T. Hong, P. Yang *et al.*, Magnetic asymmetry induced anomalous spin-orbit torque in IrMn, Phys. Rev. B **101**, 184403 (2020).

[18] Y. Liu, Y. Liu, M. Chen, S. Srivastava, P. He, K. L. Teo, T. Phung, S. H. Yang, and H. Yang, Current-Induced Out-Of-Plane Spin Accumulation on the (001) Surface of the $IrMn_3$ Antiferromagnet, Phys. Rev. Appl. **12**, 064046 (2019).

[19] H. Bai, X. F. Zhou, H. W. Zhang, W. W. Kong, L. Y. Liao, X. Y. Feng, X. Z. Chen, Y. F. You, Y. J. Zhou, L. Han *et al.*, Control of spin-orbit torques through magnetic symmetry in differently oriented noncollinear antiferromagnetic Mn_3Pt, Phys. Rev. B **104**, 104401 (2021).

[20] Y. You, H. Bai, X. Feng, X. Fan, L. Han, X. Zhou, Y. Zhou, R. Zhang, T. Chen, F. Pan *et al.*, Cluster magnetic octupole induced out-of-plane spin polarization in antiperovskite antiferromagnet, Nat. Commun. **12**, 6524 (2021).

[21] K. Kondou, H. Chen, T. Tomita, M. Ikhlas, T. Higo, A. H. MacDonald, S. Nakatsuji, and Y. C. Otani, Giant field-like torque by the out-of-plane magnetic spin Hall Effect in a topological antiferromagnet, Nat. Commun. **12**, 6491 (2021).

[22] X. Wang, M. T. Hossain, T. R. Thapaliya, D. Khadka, S. Lendinez, H. Chen, M. F. Doty, M. B. Jungfleisch, S. X. Huang, X. Fan *et al.*, Spin currents with unusual spin orientations in noncollinear Weyl antiferromagnetic Mn_3Sn, Phys. Rev. Mater. **7**, 034404 (2023).

[23] W. Zhang, W. Han, S. H. Yang, Y. Sun, Y. Zhang, B. Yan, and S. S. P. Parkin, Giant facet-dependent spin-orbit torque and spin Hall conductivity in the triangular antiferromagnet $IrMn_3$, Sci. Adv. **2**, e1600759 (2016).

[24] J. Holanda, H. Saglam, V. Karakas, Z. Zang, Y. Li, R. Divan, Y. Liu, O. Ozatay, V. Novosad, J. E. Pearson *et al.*, Magnetic Damping Modulation in $IrMn_3/Ni_{80}Fe_{20}$ via the Magnetic Spin Hall Effect, Phys. Rev. Lett. **124**, 087204 (2020).

[25] J. C. R. Sánchez, L. Vila, G. Desfonds, S. Gambarelli, J. P. Attané, J. M. De Teresa, C. Magén, and A. Fert, Spin-to-Charge conversion using Rashba coupling at the interface between nonmagnetic materials, Nat. Commun. **4**, 2944 (2013).

[26] Q. Shao, G. Yu, Y. W. Lan, Y. Shi, M. Y. Li, C. Zheng, X. Zhu, L. J. Li, P. K. Amiri, and K. L. Wang, Strong Rashba-Edelstein effect-induced spin-orbit torques in monolayer transition metal dichalcogenide/ferromagnet bilayers, Nano Lett. **16**, 7514 (2016).

[27] L. Chen, M. Decker, M. Kronseder, R. Islinger, M. Gmitra, D. Schuh, D. Bougeard, J. Fabian, D. Weiss, and C. H. Back, Robust spin-orbit torque and spin-galvanic effect at the Fe/GaAs (001) interface at room temperature, Nat. Commun. **7**, 13802 (2016).

[28] S. C. Baek, V. P. Amin, Y. Oh, G. Go, S. Lee, G. Lee, K. Kim, M. D. Stiles, B. Park, and K. Lee, Spin currents and spin – orbit torques in ferromagnetic trilayers, Nat. Mater. **17**, 509 (2018).

[29] X. R. Wang, Anomalous spin Hall and inverse spin Hall effects in magnetic systems, Commun. Phys. **4**, 55 (2021).

[30] T. C. Chuang, D. Qu, S. Y. Huang, and S. F. Lee, Magnetization-Dependent spin Hall effect in a perpendicular magnetized film, Phys. Rev. Res. **2**, 032053(R) (2020).

[31] A. Yagmur, S. Sumi, H. Awano, and K. Tanabe, Magnetization-Dependent inverse spin Hall effect in compensated ferrimagnet TbCo Alloys, Phys. Rev. B **103**, 214408 (2021).

[32] Q. Fu, L. Liang, W. Wang, L. Yang, K. Zhou, Z. Li, C. Yan, L. Li, H. Li, and R. Liu, Observation of nontrivial spin-orbit torque in single-layer ferromagnetic metals, Phys. Rev. B **105**, 224417 (2022).

[33] T. Jungwirth, X. Marti, P. Wadley, and J. Wunderlich, Antiferromagnetic spintronics, Nat. Nanotechnol. **11**, 231 (2016).

[34] V. Baltz, A. Manchon, M. Tsoi, T. Moriyama, T. Ono, and Y. Tserkovnyak, Antiferromagnetic spintronics, Rev. Mod. Phys. **90**, 015005 (2018).

[35] Y. You, X. Chen, X. Zhou, Y. Gu, R. Zhang, F. Pan, and C. Song, Anomalous Hall effect–like behavior with in-plane magnetic field in noncollinear antiferromagnetic Mn_3Sn Films, Adv. Electron. Mater. **5**, 1800818 (2019).

[36] L. Liu, T. Moriyama, D. C. Ralph, and R. A. Buhrman, Spin-Torque Ferromagnetic Resonance Induced by the Spin Hall Effect, Phys. Rev. Lett. **106**, 036601 (2011).

[37] C. F. Pai, Y. Ou, L. H. Vilela-Leão, D. C. Ralph, and R. A. Buhrman, Dependence of the efficiency of spin Hall torque on the transparency of Pt/ferromagnetic layer interfaces, Phys. Rev. B **92**, 064426 (2015).

[38] See Supplemental Material at http://link.aps.org/supplemental/10.1103/PhysRevB.107.184427 for more details regarding the antisymmetric line shape V_{A} and its fitting as a function of φ_H; the modulation of exchange bias by the field annealing; the 3D structure of magnetic mirror M' and cluster magnetic octupole T in $IrMn_3$; and the generation of the interfacial out-of-plane spin polarization.

[39] M. T. Suzuki, T. Koretsune, M. Ochi, and R. Arita, Cluster multipole theory for anomalous Hall effect in antiferromagnets, Phys. Rev. B **95**, 094406 (2017).

[40] H. Tsai, T. Higo, K. Kondou, T. Nomoto, A. Sakai, A. Kobayashi, T. Nakano, K. Yakushiji, R. Arita, S. Miwa *et al.*, Electrical manipulation of a topological antiferromagnetic state, Nature (London) **580**, 608 (2020).

[41] T. Higo, K. Kondou, T. Nomoto, M. Shiga, S. Sakamoto, X. Chen, D. Nishio-Hamane, R. Arita, Y. Otani, S. Miwa *et al.*, Perpendicular full switching of chiral antiferromagnetic order by current, Nature (London) **607**, 474 (2022).

[42] H. Kurebayashi, J. Sinova, D. Fang, A. C. Irvine, T. D. Skinner, J. Wunderlich, V. Novák, R. P. Campion, B. L. Gallagher, E. K. Vehstedt *et al.*, An antidamping spin-orbit torque originating from the Berry curvature, Nat. Nanotechnol. **9**, 211 (2014).

[43] H. Saglam, J. C. Rojas-Sanchez, S. Petit, M. Hehn, W. Zhang, J. E. Pearson, S. Mangin, and A. Hoffmann, Independence of spin-orbit torques from the exchange bias direction in $Ni_{81}Fe_{19}$/IrMn bilayers, Phys. Rev. B **98**, 094407 (2018).

[44] R. Yanes, J. Jackson, L. Udvardi, L. Szunyogh, and U. Nowak, Exchange Bias Driven by Dzyaloshinskii-Moriya Interactions, Phys. Rev. Lett. **111**, 217202 (2013).

[45] J. C. Slonczewski, Current-Driven excitation of magnetic multilayers, J. Magn. Magn. Mater. **159**, L1 (1996).

[46] W. Wang, T. Wang, V. P. Amin, Y. Wang, A. Radhakrishnan, A. Davidson, S. R. Allen, T. J. Silva, H. Ohldag, D. Balzar *et al.*, Anomalous spin–orbit torques in magnetic single-layer films, Nat. Nanotechnol. **14**, 819 (2019).